Proceedings RootS25
3rd International Workshop on Soil-Vegetation-Atmosphere Interaction
Boldrin D, Cecconi M, Cotecchia F, Leung A, Pedone G, Perrini P, Romero E, Tagarelli V, Zdravković L (eds)
ISSN: 3107-300X

doi: doi.org/10.53243/RootS2025-6

Challenges and insights from root segmentation in X-ray computed tomography data of *Robinia pseudoacacia*

I. Sarhangi Fard[1], M. Wiebicke[1], M. Milatz[1], R. Hänsch[2]

[1]*Institute of Geomechanics and Geotechnical Engineering, Technische Universität Braunschweig, Braunschweig, Germany*

[2]*Institute of Plant Biology, Stress Physiology and Bioimaging, Technische Universität Braunschweig, Braunschweig, Germany*

ABSTRACT: *Robinia pseudoacacia* is a nitrogen-fixing legume tree native to eastern North America, valued for its rapid growth, drought tolerance, durable timber, and suitability as a resilient urban tree. Through symbiosis relationship with Rhizobia bacteria, which reside in root nodules and convert atmospheric nitrogen into a plant-usable form, it thrives in nutrient-poor soils. However, little is known about how this symbiosis influences root system architecture (RSA). High-resolution X-ray computed tomography was used to investigate how RSA develops in response to symbiotic nitrogen fixation in nutrient-poor sand conditions. Robinia plants, genetically identical clones of *Robinia*, were initially grown in agar and later potted in poorly graded sand to enable the identification of individual grains. Rhizobia were introduced after initial growth to establish nitrogen-fixing symbiosis. By scanning the plants before and after inoculation, we can track the development of RSA.
A major challenge is image segmentation: root tissue and pore water exhibit similar X-ray attenuation, and nodules often fuse with fine root hairs. These factors hinder clean separation of the four present phases: Soil, root, water, and air. This study therefore focuses on developing segmentation workflows to achieve robust segmentation for further studies.

Keywords: Soil vegetation; X-ray CT; Image analysis; Root morphology

1 INTRODUCTION

Soil bioengineering with roots is regarded as an environmentally friendly approach to slope stabilization (Ni et al., 2018). A well-recognised influence of roots on slope stability is their role in providing mechanical reinforcement by increasing the tensile and shear strength of the soil, while also inducing beneficial hydraulic effects such as increasing soil matric suction through root water uptake (Masi et al., 2021; Ni et al., 2018).

For geotechnical applications, quantifying the microstructural changes in soil induced by root growth is essential to understand root-soil interactions (Kemp et al., 2022). X-ray micro-computed tomography (μCT), as a non-invasive approach, has been used progressively to quantify soil-root morphology and volumetric fraction metrics over time (Anselmucci et al., 2021; Kemp et al., 2022) and is known as a powerful method for in situ quantification of root system architecture (RSA) (Gao et al., 2019).

Effective CT image-based analysis of unsaturated, vegetated soils requires accurate, reliable multiphase segmentation of soil grains, roots, pore water and pore air, which can be achieved using either classical or machine learning-based approaches (Jiang et al., 2025).

However, multiphase segmentation is challenging due to partial volume effects, the similar X-ray attenuation of different phases (especially water, roots, and organic matter), which yields low greyscale contrast (Xu et al., 2018), and results in segmentation uncertainty (Jiang et al., 2025). Metzner et al. (2015) found that high water content especially near the pot bottom, degrades CT root segmentation.

Unlike deterministic segmentation, which assigns a single, definite prediction to each pixel/voxel and hides boundary ambiguity, probabilistic segmentation assigns per pixel/voxel class probabilities that capture segmentation uncertainty (Krygier et al., 2021).

In this study, we selected *Robinia pseudoacacia,* which has a fibrous root system, to investigate root-system morphology due to its drought tolerance, fast growth, adaptability to degraded soils, high biomass yield, durable wood, and associated environmental and economic benefits (Ciuvăț et al., 2022). By scanning the same specimen in wet and dry states, the effects of water content on μCT image-based analysis were assessed. Using probabilistic segmentation, the root phase was segmented in both scans and root volumetric fraction (θ_r) and specific surface area (SSA) were compared to quantify segmentation uncertainty.

2 MATERIALS AND METHODS

2.1 Sample preparation

Robinia plants germinated by the Institute of Plant Biology at Technical University of Braunschweig were transferred to cylindrical containers with 100 mm height, 68 mm inner diameter, and 2 mm wall thickness made of polypropylene homopolymer (PP-H). The cylinders were filled with a quartz sand with a mean grain size (D_{50}) of 0.76 mm and particle sizes ranging from 0.63 to 2.0 mm based on standard sieve analysis. The samples were watered roughly every 24 h by adding water to trays beneath the pots, allowing uptake through five drainage holes; the water volume was adjusted so the trays dried within 24 h. Cool-running LED lamps above the plants provided a 16 h light /8 h dark cycle to simulate sunlight. Plants were inoculated once with Rhizobia bacteria by pipetting 1 mL of suspension around the root zone, followed by 5 mL of water to transport bacteria into the substrate. Thereafter, a nitrogen-free nutrient solution was applied to support plant growth under symbiotic conditions. X-ray micro-computed tomography (µCT) was employed to investigate the RSA of Robinia plants. In addition to the regular scans during the measurement campaign, one sample was scanned under moist conditions (degree of saturation $S_r = V_{water}/V_{pores} \approx 0.873$), after which watering was ceased for three days to allow drying ($s_r \approx 0.0$) in order to obtain a subsequent scan under dry sand conditions.

2.2 Acquisition, preprocessing and segmentation of X-ray computed tomography images

The µCT images were acquired using an EasyTom 160-150 nano/micro-CT scanner (RX Solutions, France) at the Institute of Applied Mechanics (IAM), TU Braunschweig. Scans were performed at a voltage of 150 kV and a current of 500 µA. 3D volumes were reconstructed using filtered back projection in RX Solutions' reconstruction and analysis software X-Act. Full-field scans of the entire pot volume were acquired, with a voxel size of 59 µm. Raw 16-bit greyscale images (1705 × 1469 × 1469 voxels) were processed to extract the plant RSA. To reduce computational cost, the volumes were converted to 8-bit in Fiji (Schindelin et al., 2012), and inter-scan misalignment between wet and dry stacks was corrected by rigid 3D registration using the Software for the Practical Analysis of Materials (SPAM) toolkit (Stamati et al., 2020).

CT images were preprocessed prior to segmentation. Denoising was performed using the GPU-accelerated Non-Local Means (NLM) filter in Avizo (Avizo, 2024) to reduce intra-phase noise while preserving edges (Jiang et al., 2025), with spatial standard deviation of 5 and a search window of 10 px. To enhance phase boundaries, an Unsharp Masking (USM) filter (blur radius = 1.5, mask weight = 0.7) was applied (Jiang et al., 2025). Then, the cylindrical pot wall was removed to process only the interior. Both steps were performed in Fiji (Schindelin et al., 2012).

After pre-processing, the four phases, root, soil, water, and air, were segmented using the open-source software Ilastik (Berg et al., 2019), which enables interactive learning and classification of image data.

First, the Pixel Classification workflow in Ilastik was used. Training datasets were created by manually labeling pixels from each phase (soil, root, air, and water), while the outputs of various image filters (e.g., Gaussian smoothing, Laplacian of Gaussian, and others) were used as features for the Random Forest classifier. The classifier was then trained on these inputs, resulting in the generation of probability maps for all phases. In these maps, every voxel is assigned a class-specific probability *P* (e.g., root, air, soil, water), representing the classifier's confidence that the voxel belongs to that class.

Second, the probability maps were then used as input for the Object Classification workflow in Ilastik. In this step, connected objects were extracted from the probability maps by applying smoothing and thresholding, and a comprehensive set of object-level features was calculated. These features include the intensity distribution within each object and its neighbourhood, as well as morphological descriptors. Using interactive annotations, objects were assigned to different classes, and the trained object-level classifier enabled refinement of segmentation (Berg et al., 2019).

2.3 Quantitative metrics for root segmentation

For each scan, the Ilastik root-probability map was thresholded at α = 0.3, 0.5, and 0.7 to obtain binary root masks. Here, α denotes the threshold for the root class in the probability map (voxels with $P_{\text{root}} \geq \alpha$ are labeled as root). The region of interest (ROI) was a fixed subvolume (290 × 340 × 410 voxels) containing the main root axis and fine roots. Isolated components smaller than 1000 voxels were removed in both tomographies (wet and dry) and for all α-thresholded masks before quantification to suppress noise and exclude disconnected fine hair-root fragments. Two metrics were reported: the root volumetric fraction and the specific surface area (SSA = root surface area/root volume) computed in Avizo (Jiang et al., 2025, Avizo, 2024). The root volumetric fraction (θ_r) was calculated as the ratio of root-labelled voxels to the total voxels in the ROI. The relative error (RE) in this study is defined as $(\upsilon_i - \upsilon_{\text{ref}})/\upsilon_{\text{ref}}$, with υ_{ref} set to the dry scan at α = 0.5, where υ_i is the value of metric *i* (either SSA or θ_r).

3 RESULTS AND DISCUSSION

Figures 1a and b show the segmented root systems from the wet and dry scans obtained by thresholding the root

probability map at α = 50%. Figures 1c–h compare the segmented roots from the wet and dry scans at α = 0.3, 0.5, and 0.7. In the wet scan, numerous small fragments and locally thickened surfaces appear as false-positive root voxels caused by overlap in X-ray attenuation (greyscale) between roots and water-filled pores and partial-volume mixing at the root–pore interface; these false-positive voxels diminish as α increases. In the dry scan, the contrast between the root and surroundings increases, and the segmentation retains the main root segments while eliminating many false-positive voxels. From the literature, fine hair roots exhibit higher segmentation uncertainty than coarse roots (Jiang et al., 2025); therefore, increasing α can falsely remove true hair-root voxels in both wet and dry scans, with a stronger effect in the wet scan due to reduced greyscale contrast between roots and water.

Figure 2 represents the root volumetric fraction (θ_r) and specific surface area (SSA) as functions of α. Increasing the root-probability threshold reduced both metrics in both scans; from α = 0.3 to 0.7, θ_r changed by about −39% (wet) and −20% (dry), while SSA changed by about −41% (wet) and −22% (dry). The decrease was markedly stronger for both metrics in the wet scan, indicating greater α-sensitivity as many low-confidence voxels were reassigned to other phases at higher α; the steeper drop in SSA is consistent with excluding spurious fragments and high-curvature surface voxels arising from greyscale overlap between roots and water,

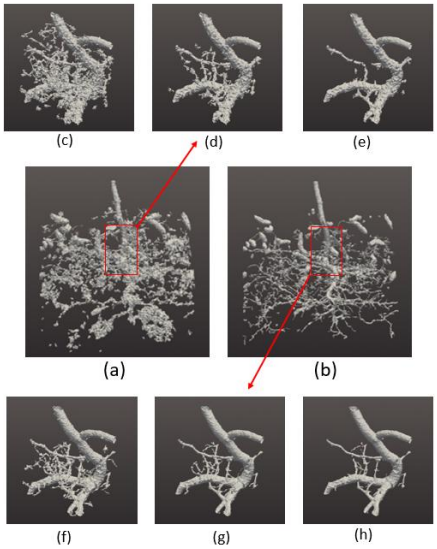

Figure 1. Central panel: segmented roots at α = 0.5: (a) wet scan; (b) dry scan. Top row: wet subvolume across α: (c) α = 0.3, (d) α = 0.5, (e) α = 0.7. Bottom row: dry subvolume across α: (f) α = 0.3, (g) α = 0.5, (h) α = 0.7

yielding a smoother root surface at higher thresholds. The dry scan showed a smaller decline and consistently lower metrics across α, indicating that drying the sample suppressed the root–water greyscale overlap that inflates apparent root volume and therefore fewer ambiguous boundary voxels near the root–pore interface; correspondingly, SSA was more weakly α-dependent, reflecting smoother surface and reduced sensitivity to threshold after drying.

Figure 4 uses the dry scan at α = 0.5 as a baseline and shows the relative error for both metrics to quantify their sensitivity to α. At α = 0.3, the wet scan departs strongly from the baseline ($RE_{\theta_r} \approx 0.68$, $RE_{SSA} \approx 0.63$), whereas the dry scan is closer ($RE_{\theta_r} \approx 0.15$, $RE_{SSA} \approx 0.22$). At α = 0.5, the dry series is zero by definition and the wet series remains positive ($RE_{\theta_r} \approx 0.22$, $RE_{SSA} \approx 0.07$). By α = 0.7, all curves approach the baseline (wet: $RE_{\theta_r} \approx 0.03$, $RE_{SSA} \approx -0.03$; dry: $RE_{\theta_r} \approx -0.08$, $RE_{SSA} \approx -0.05$). Overall, increasing α drives both series towards the baseline, with the wet scan showing the largest deviations at low α, indicating greater sensitivity to thresholding. Negative RE values (e.g., at α = 0.7) mean that, relative to the baseline, the segmentation yields lower measured root volume and surface area because higher α excludes more ambiguous boundary voxels from the root label, reassigning them to non-root phases.

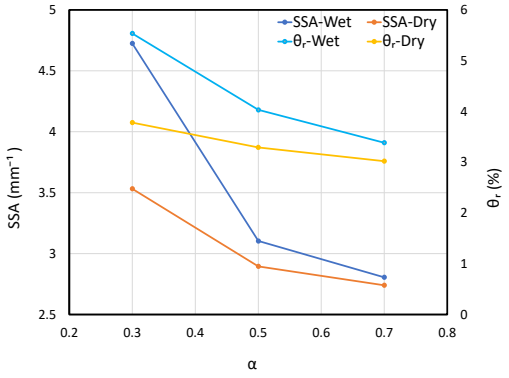

Figure 2. Comparison of root volumetric fraction (θ_r) and specific surface area (SSA) as a function of root probability threshold α for wet and dry scans

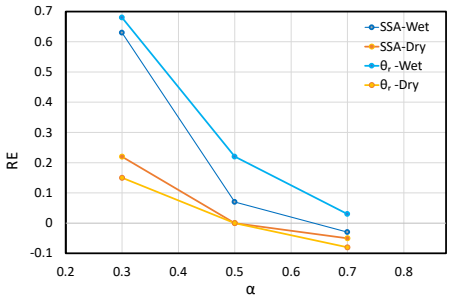

Figure 3. Relative error (RE) of root volumetric fraction (θ_r) and specific surface area (SSA) versus the root-probability threshold α; the results for the dry scan at alpha=0.5 serve as a reference

Based on previous studies, SSA and θ_r are key descriptors of soil-root interactions. Greater SSA, especially via root hairs, expands root-soil contact and the absorptive surface, thereby enhancing water and nutrient uptake (Goss et al., 1993; Duddek et al., 2023). The literature shows that θ_r is an important parameter for evaluating soil hydraulic properties. Ng et al. (2016) proposed a new, simple model to predict how plant roots modify the soil-water retention curve (SWRC) using a single root parameter, the root volume ratio (R_v) which

is defined as the total volume of roots per unit volume of soil. Hydraulic conductivity is affected by root biomass: fine roots can lower permeability by blocking pores, while coarse roots can increase it by rearranging soil particles (Jiang et al., 2025).

From the results, in the wet scan, the RE values change substantially more with increasing α for both metric curves compared with the dry scan. This greater segmentation uncertainty, driven by the presence of water, reduces root-segmentation accuracy and can lead to erroneous soil–root interaction calculations and misinterpretation. Consistent with our results, prior work shows that lower saturation improves root-phase segmentation accuracy in CT image-based analysis of vegetated soils. (Jiang et al., 2025).

4 CONCLUSIONS

Accurate plant root segmentation is essential for reliable estimates of root metrics such as volumetric fraction (θ_r) and morphological properties (e.g., SSA). These metrics underpin the interpretation of the hydromechanical effects of vegetation; when segmentation uncertainty is high, soil–root interactions are mischaracterized and interpretations become unreliable. Using probabilistic segmentation as a machine-learning approach, root-segmentation uncertainty was quantified in X-ray CT images of a vegetated sample in the wet and dry states. Across α = 0.3–0.7, the wet-soil scan showed higher values and a stronger α-dependence for θ_r and SSA, indicating greater segmentation uncertainty, whereas these metrics in the dry scan were lower and notably less sensitive to α. These observations are consistent with improved root–matrix contrast in the dry state and reduced segmentation uncertainty, yielding more robust estimates of root volume and surface area. Since hair roots are more susceptible to segmentation uncertainty than coarse root sections, increasing α resulted in their progressive loss in both scans; the effect was magnified in the wet scan. Minor wet–dry differences may also reflect root shrinkage after drying; this was not quantified in this study and should be considered when interpreting absolute values in future work. The analysis was limited to two metrics, and two saturation states. Extending to complementary morphology indices and more variations of saturation, respectively, would further generalise the findings.

5 REFERENCES

Anselmucci, F., Andò, E., Viggiani, G., Lenoir, N., Arson, C., Sibille, L. 2021. Imaging local soil kinematics during the first days of maize root growth in sand, *Scientific Reports* **11**(1), 1–13.

Berg, S., Kutra, D., Kroeger, T., Straehle, C.N., Kausler, B.X., Haubold, C., Schiegg, M., Ales, J., Beier, T., Rudy, M., Eren, K., Cervantes, J.I., Xu, B., Beuttenmueller, F., Wolny, A., Zhang, C., Koethe, U., Hamprecht, F.A., Kreshuk, A. 2019. ilastik: interactive machine learning for (bio)image analysis, *Nature Methods* **16**, 1226–1232.

Ciuvăț, A.L., Abrudan, I.V., Ciuvăț, C.G., Marcu, C., Lorenț, A., Dincă, L., Szilard, B. 2022. Black locust (Robinia pseudoacacia L.) in Romanian forestry, *Diversity* **14**, 780.

Duddek, P., Ahmed, M.A., Javaux, M., Vanderborght, J., Lovric, G., King, A., Carminati, A. 2023. The effect of root hairs on root water uptake is determined by root–soil contact and root hair shrinkage, *New Phytologist* **239**(3), 1172–1186.

Gao, W., Schlüter, S., Blaser, S.R.G.A., Shen, J., Vetterlein, D. 2019. A shape-based method for automatic and rapid segmentation of roots in soil from X-ray computed tomography images: Rootine, *Plant and Soil* **441**, 643–655.

Goss, M.J., Miller, M.H., Bailey, L.D., Grant, C.A. 1993. Root growth and distribution in relation to nutrient availability and uptake, *European Journal of Agronomy* **2**(2), 57–67.

Jiang, Z., Leung, A.K., Liu, J. 2025. Segmentation uncertainty of vegetated porous media propagates during X-ray CT image-based analysis, *Plant and Soil* **511**, 969–995.

Kemp, N., Angelidakis, V., Luli, S., Nadimi, S. 2022. How do roots interact with layered soils? *Journal of Imaging* **8**(1), 5.

Krygier, M.C., LaBonte, T., Martinez, C., Norris, C., Sharma, K., Collins, L.N., Mukherjee, P.P., Roberts, S.A. 2021. Quantifying the unknown impact of segmentation uncertainty on image-based simulations, *Nature Communications* **12**, 5414.

Masi, E.B., Segoni, S., Tofani, V. 2021. Root reinforcment in slope stability models: a review, *Geosciences* **11**, 212.

Metzner, R., Eggert, A., van Dusschoten, D., Pflugfelder, D., Gerth, S., Schurr, U., Uhlmann, N., Jahnke, S. 2015. Direct comparison of MRI and X-ray CT technologies for 3D imaging of root systems in soil: potential and challenges for root trait quantification, *Plant Methods* **11**, 17.

Ni, J.J., Leung, A.K., Ng, C.W.W., Shao, W. 2018. Mod elling hydro-mechanical reinforcements of plants to slope stability, *Computers and Geotechnics* **95**, 99–109.

Ng, C.W.W., Ni, J.J., Leung, A.K., Wang, Z.J. 2016. A new and simple water retention model for root-permeated soils, *Geotechnique Letters* **6**, 82–86.

Schindelin, J., Arganda-Carreras, I., Frise, E., Kaynig, V., Longair, M., Pietzsch, T., Preibisch, S., Rueden, C., Saalfeld, S., Schmid, B., Tinevez, J.-Y., White, D.J., Hartenstein, V., Eliceiri, K., Tomancak, P., Cardona, A. 2012. Fiji: an open-source platform for biological-image analysis, *Nature Methods* **9**, 676–682.

Stamati, O., Andò, E., Roubin, E., Cailletaud, R., Wiebicke, M., Pinzon, G., Couture, C., Hurley, R.C., Caulk, R., Caillerie, D., Matsushima, T., Bésuelle, P., Bertoni, F., Arnaud, T., Ortega Laborin, A., Rorato, R., Sun, Y., Tengattini, A., Okubadejo, O., Colliat, J.-B., Saadatfar, M., Garcia, F.E., Papazoglou, C., Vego, I., Brisard, S., Dijkstra, J., Birmpilis, G. 2020. SPAM: software for practical analysis of materials, *Journal of Open Source Software* **5**(51), 2286.

Thermo Fisher Scientific. 2024. *Avizo (Version 2024.0)*, Waltham, MA, USA.

Xu, Z., Valdes, C., Clarke, J. 2018. Existing and potential statistical and computational approaches for the analysis of 3D CT images of plant roots, *Agronomy* **8**(5), 71.